Chapter 22
Response Reductions in Base-Isolated Liquid Storage Tank Under Far and Near Field Seismic Excitations

Sourabh Vern, Sunita Tolani, Shiv Dayal Bharti, and Mahendra Kumar Shrimali

22.1 Introduction

Concrete ground supporting LST is one of the important and widespread civil facility infrastructures that has been used in the production and transportation of numerous materials and products in the oil refining, chemical industry, nuclear power station, wastewater plant, sewage treatment plant, and railway industries. The collapse of these systems leads to serious hazards in the regional environment and also have a long-term impact. Control mechanisms are needed to protect against the failure of LSTs even for the extreme earthquake levels. Damages in the liquid storage tanks during seismic events were observed.

For long-term and effective control of the responses in LSTs, its behavior needs a profound understanding. The structural responses of the LSTs under the earthquake excitations are different from normal load-bearing structures, as the interaction between two different media is involved, i.e., tank and fluid. Thus, to simplify the understanding of the LSTs, it is divided into two major components, i.e., impulsive and convective. The impulsive component is due to the rigid behavior of the LSTs wall and the stationary fluid mass which behaves like solid mass during the earthquake event.

The most common lumped mass approach was presented by Housner [1, 2]; by extending Housner's lumped mass approach, several authors studied the behavior of the LSTs under harmonic and irregular excitations [3, 4].

As the experimental approach gains attention of the researchers, the analytical results and numerical results for the harmonic motions were verified by many authors [5, 6]. Due to the infrastructural limitations of the experimental approach and the inability of the numerical and analytical approaches in solving and capturing the nonlinear behavior of the fluid, finite element method (FEM) quickly gained attention as an effective and computationally less expensive method [7–10]. In the recent

S. Vern · S. Tolani · S. D. Bharti · M. K. Shrimali (✉)
National Centre for Disaster Mitigation and Management, MNIT Jaipur, Jaipur, Rajasthan, India

© The Author(s), under exclusive license to Springer Nature Singapore Pte Ltd. 2022

S. Kolathayar et al. (eds.), *Civil Engineering for Disaster Risk Reduction*, Springer Tracts in Civil Engineering, https://doi.org/10.1007/978-981-16-5312-4_22

past, Rawat et al. [11] studied the earthquake-induced sloshing and hydrodynamic pressure developed in the rigid cylindrical storage tanks with the help of commercial FEM software ABAQUS. The study showed the difference between the two different FEM approaches, namely coupled acoustic-structural (CAS) and coupled Euler–Lagrangian method (CEL). It was concluded that CAS provided the faster results with lower accuracy, whereas CEL proved to be a better option in studying the low-amplitude sloshing effect. Kirtas et al. [12] investigated the modal response of liquid storage steel tanks, and the associated prevailing frequencies in the horizontal impulsive mode of vibration are explored using earthquake recordings.

The use of base isolation in LSTs has drawn the interest of research due to the successful application of base isolation systems in the seismic regulation of many structures. Many researchers have explored thoroughly the seismic study of the base-isolated cylindrical steel LSTs [13–18].

The study of isolated LSTs for bidirectional motion under seismic excitations is comparatively smaller. Many scholars presented some of the early finite element studies [19–21]. Recently, Cheng et al. [22] studied the effect of free-surface sloshing with the help of the velocity potential function that was obtained by the superposition principle and the Navier-Stokes equation obtained by the principle of the mass conservation of the fluid movement. It was concluded that free-surface sloshing plays an important part in estimating the structural responses.

While both steel and concrete LSTs have been studied in the past for a broad range of controlling variables in the seismic response behavior study, the same is comparatively fewer for the base-isolated LSTs. In particular, the efficacy of base isolation in improving the seismic behavior under bidirectional earthquake excitation of 3D concrete LSTs has not been studied in great detail. In this article, to figure out the efficacy of base isolation in LSTs under a range of significant parametric variations, a detailed analysis of a 3D concrete base-isolated LST is performed. These include the use of base isolation in terms of (i) type of earthquake; (ii) the reduction of the various amounts of concern in response; (iii) the spillage of fluid; (iv) the seismic isolation characteristics; and (v) the direction of incidence of seismic events.

22.2 Theory

For the combination of dead and seismic loads, the concrete LST is designed. The LST base is protected by base isolators resting on the hardened surface. The laminated rubber bearing lacks the high dissipation properties of energy; thus, in the New Zealand lead core rubber bearing, a more efficient isolator device is chosen (LRB). Additional energy dissipation properties are pumped into the isolation system due to the central lead center, which results in a greater volume of the isolator system's hysteresis loop. The nonlinear behavior of the LRB isolation system (LRB) has been idealized by various models [23, 24]. Wen's bilinear hysteretic model is shown in Fig. 22.1.

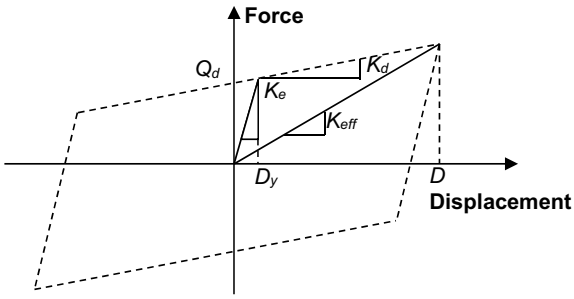

Fig. 22.1 Bilinear behavior of the LRB isolator

There are three salient parameters in the bilinear curve, namely (i) yield strength F_y; (ii) characteristic strength Q_d; and (iii) post-yield rigidity ratio (K_d/K_e or K_2/K_1). At the displacement value of zero, the characteristic strength is the intercept of force. The characteristic strength of the LRB isolator is determined by the yield strength of lead in shear, f_{py}, as shown in Eq. 22.1 for a given area of A_p.

$$Q_d = f_{py} \times A_p \tag{22.1}$$

Equation 22.2 gives the relation between the post-yield stiffness K_d and effective stiffness K_{eff} at the stated design displacement D and Q_d

$$K_d = K_{\text{eff}} - \frac{Q_d}{D} \tag{22.2}$$

The effective damping β_{eff} of the isolator is calculated for the displacement D_y by Eq. (22.3)

$$\beta_{\text{eff}} = \frac{2Q_d}{\pi D^2 K_{\text{eff}}}(D - D_y) \tag{22.3}$$

With the LRB isolator, the time history analysis of the concrete LST is very costly and poses many challenges. An eight-node linear brick element (C3D8R) is defined for the LST, with hourglass control and reduced integration scheme available in ABAQUS. The fluid is also modeled by the same brick element as the tank to grasp and mimic the sloshing in the LST. It provides a combined hourglass regulation with a factor of 0.85 to provide the brick components with fluid behavior. Because the fluid simulation takes the distortion of the mesh to a large factor, an effective mesh control technique is needed. The analysis of finite elements provides a few methods to analysis, generally known as Lagrangian and Eulerian approaches. The material will move through the defined mesh boundaries in the Eulerian analysis while preventing any distortion of the element, whereas in the Lagrangian analysis, the material stays in the closed boundaries of the elements that do not cause the elements to be strongly distorted. The arbitrary Lagrangian–Eulerian (ALE) solution is used in the current simulation of the FSI to prevent high distortion in the finite elements. The material

flow and movement caused in the mesh were controlled by the use of ALE to control the distortion in the study, resulting in a reduced disruption in the mesh. In the analysis, this lower distortion of the mesh ensures continuity. For the current case study, the ALE formulation used by the ABAQUS uses second-order advection and element center projection momentum advection that requires fewer iterations.

22.3 Numerical Study

The LST for the present study is taken up for the study of the dimension 6 m × 6 m × 4.8 m with a wall thickness of 0.3 m. The various constitutive material properties of the LST and fluid are shown in Table 22.1. For the present study of the LST, a total of five isolators are used that are attached to the rigid base. For an extensive review of the behavior of the LST under the seismic event, four different types of earthquakes are used for the nonlinear response history analysis in ABAQUS. The four different earthquakes are Kern County (1952), Parkfield (2004), Imperial Valley (1940), and Kocaeli (1999). The earthquakes are scaled to the three different PGA levels, namely 0.2 g, 0.4 g, and 0.6 g. The ratio between the horizontal components of the earthquakes is taken as 1:0.67.

For the analysis, the isolators are modeled by the connector elements which are available in the ABAQUS element library. For an effective isolator model, elasticity, damping, and bilinear behavior are selected. The connector element used in the analysis is built by Cartesian and align boundary conditions. The bottom node of the connector elements is joined to the fixed base, whereas the top node is connected to LST.

The effect of the directionality of the earthquake is an important and influential parameter that can alter the critical response in the LSTs. For the present study, five different angles of incidence are taken which are zero degrees, fifteen degrees, thirty degrees, forty-five degrees, sixty degrees, and seventy-five degrees. For base isolation of the LSTs, as there are no such recommendations for an optimum period, therefore, seven different isolation time periods are used to find out the optimum time period for response control. Different isolation properties are shown in Table 22.2.

Table 22.1 Properties of 3D square tank and fluid

Concrete	Fluid (water)
Modulus of elasticity, E_s = 24.86 GPa	Density, $\rho_w = 983.204$ kg/m^3
Density, $\rho_s = 2450$ kg/m^3	Equation of state: $c_0 = 1450$, $s = 0$, $\gamma_0 = 0$
Poisson's ratio, $\upsilon = 0.17$	Dynamic viscosity = 0.001 N s/m^2

Table 22.2 Properties of isolators designed for different time periods

Isolation period, T_{iso} (s)	Effective stiffness, K_{eff} (kN/m)	Elastic stiffness, K_e (kN/m)	Post-yield stiffness ratio, $\gamma = K_d/K_e$	Characteristic strength, Q_d (kN)
0.85	2250	17,690	0.09	30
1.0	1600	12,780	0.09	25
1.5	725	5700	0.09	18
2.0	400	3200	0.09	16
2.25	320	2525	0.09	14
2.5	250	1980	0.09	12
3.0	180	1420	0.09	9.5

22.4 Results and Discussions

The effectiveness of the LRB isolator for the LSTs under seismic ground motion is evaluated against the effective isolation period, type of ground motion, peak ground acceleration (PGA), and angle of incidence. The response quantities under investigation are shear force, overturning moment, hydrodynamic pressure, and sloshing height.

22.4.1 Shear Force

Figure 22.2 shows the effect of the variation of the effective isolation period on the shear force. It is seen from the estimates that with the increase in the T_b, the decrease in the shear force usually increases. However, after the value of $T_b = 2$ s, the rate of increase in the percentage reduction of the shear force is not very important. The curve becomes almost horizontal after a value of $T_b = 2.5$ s. The overall decrease in effective stress is 75% of the order.

For various types of earthquakes, the pattern variation of the percentage reduction of shear force with T_b is different before $T_b = 1.5$ s; after that, for all types of earthquakes, the pattern of variation is observed to be almost the same.

The variation between the percentage reduction of the shear force and the angle of earthquake incidence is seen in Fig. 22.3. The figure reveals that the percentage of reduction in shear force stays the same for all angles of incidence for most earthquakes, beginning from 15° to 75°, except for the Imperial Valley earthquake, which shows further reduction at 15° and 60°, but the percentage reduction rise is not very important.

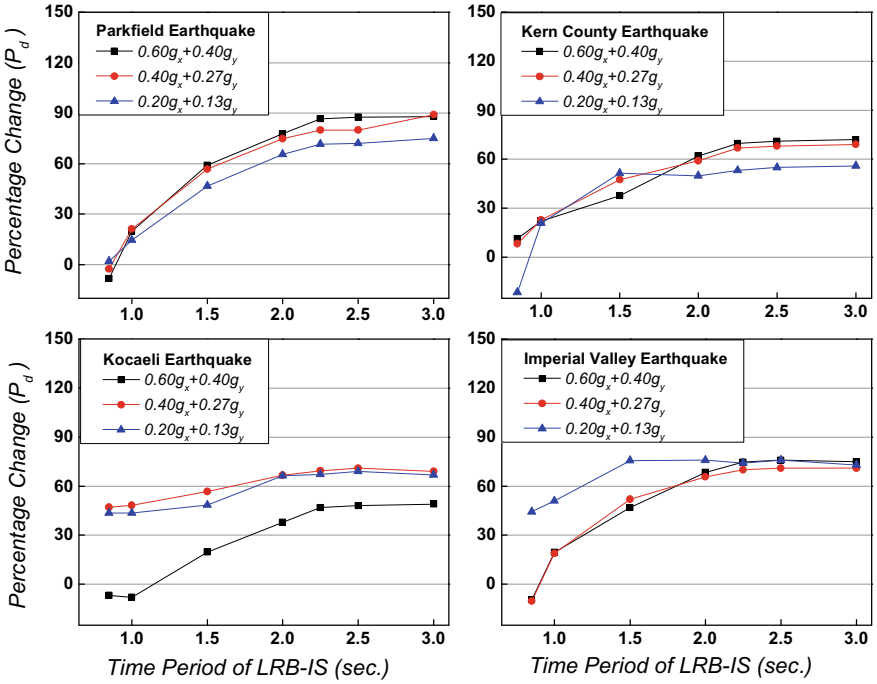

Fig. 22.2 Variation of percentage reduction in shear force with the time period of LRB isolator

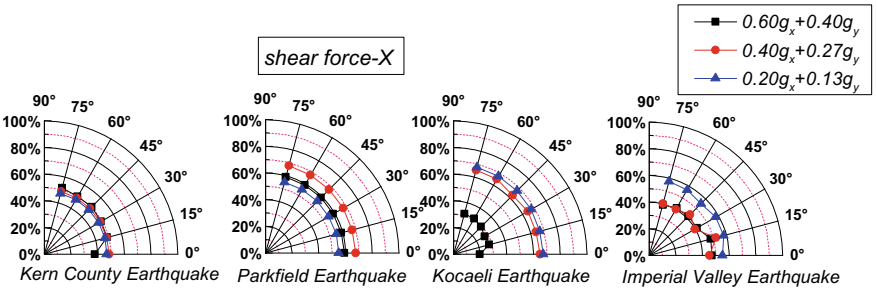

Fig. 22.3 Variation of percentage reduction in shear force with the angle of incidence

22.4.2 Overturning Moment

Figure 22.4 shows the effect of the variation of the effective isolation period on the overturning moment with the effective time period of the isolator. From Fig. 22.4, it can be seen that after the particular value of the isolator time period, the responses are no longer get affected. Like the pattern in the shear force reduction, the overturning moment shows similar behavior. Except for the Parkfield earthquake (near field with

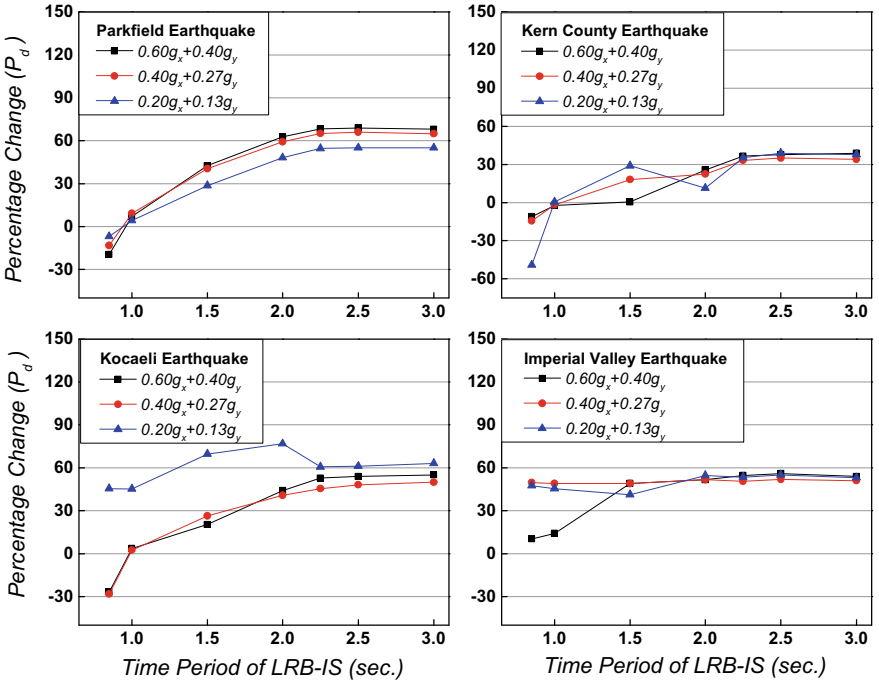

Fig. 22.4 Variation of percentage reduction in the overturning moment with the time period of LRB isolator

directivity effect), the rate of change in the reduction in response is very little in the overturning moments, and the maximum percentage reduction is on the order of 70–75%. The pattern of variation of the percentage reduction of the overturning moments with the T_b is distinct for different types of earthquakes up to $T_b = 1.5$ s; after that, the pattern of variation for all types of earthquakes does not change substantially.

The variations of the percentage decrease in the overturning moments with different PGAs do not show any definite pattern, like for the instance of the shear forces. As regards the difference of the reduction of the overturning moment with the angle of incidence, the percentage decrease, as shown in Fig. 22.5, is not sensitive to the variation of the angle of incidence of earthquake for all the cases under examination.

22.4.3 Hydrodynamic Pressure

The effect of the variation of the isolator time period on the reduction of the hydrodynamic pressure can be seen from Fig. 22.6. It can be seen from the figure that reduction in hydrodynamic pressure reaches a constant reduction value after a $T_b = 2.5$ s. In

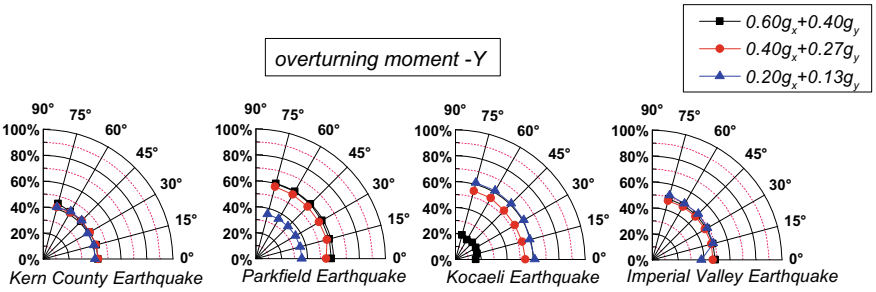

Fig. 22.5 Variation of percentage reduction in the maximum overturning moment with the angle of incidence

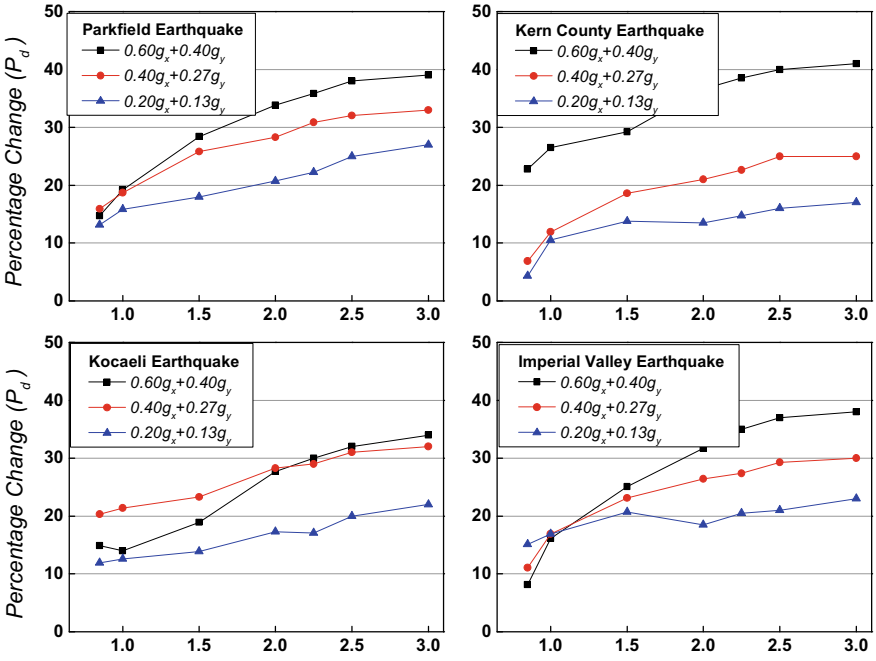

Fig. 22.6 Variation of percentage amplification in sloshing height with the time period of LRB isolator

comparison, it is shown that the magnitude of the difference depends to a greater degree on the type of earthquake relative to other response quantities. Compared to other response quantities, the influence of PGA on hydrodynamic pressure reduction is also prominent.

The effect of the angle of incidence of the earthquake on the reduction of the hydrodynamic pressure can be from Fig. 22.7. It can be seen from the figure that at an angle of incidence of fifteen degrees, the reduction is slightly more, whereas at an

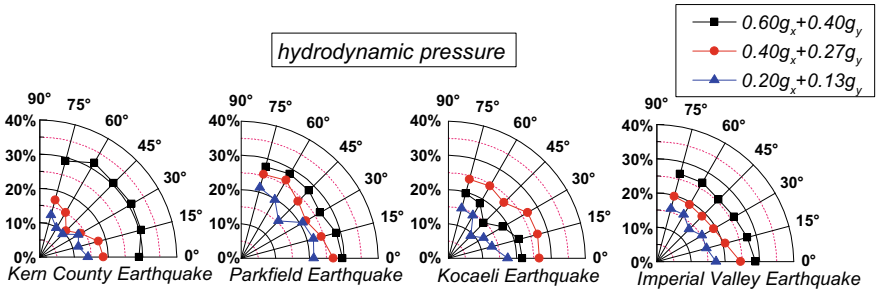

Fig. 22.7 Variation of percentage reduction in maximum hydrodynamic pressure with the angle of incidence

angle of incidence of forty-five degrees in all four cases of earthquakes, percentage reduction becomes reduced. Again, the effect of the PGA variation can be seen in the results of the angle of incidence variations.

22.4.4 Sloshing Height

In the base-isolated LSTs, the sloshing height is amplified in comparison to the other response quantities. The variation of the sloshing height percentage amplification with the effective time period (T_b) for various earthquake types is seen in Fig. 22.8. It can be seen from the figure that as the isolator time period is increased, the amplification in the sloshing height becomes constant, and even after the value of $T_b = 2$ s, there is a very small amplification in the response. The maximum amplification in the sloshing height is for the Kern County earthquake which is a far field earthquake. It can also be seen from the figure that the effect of the PGA on the amplification is also significant.

The effect of the angle of incidence of the earthquake on the amplification of the sloshing height can be seen in Fig. 22.9. It can be seen from the figure that the angle of incidence of the earthquake has little effect on the variation of the amplification in the sloshing height. The amplification in the sloshing height gets lesser as the angle of incidence of earthquake reaches the range of thirty to sixty degrees. The maximum variation of amplification can be seen for the Kocaeli earthquake which is a near field earthquake with fling step effect, whereas the minimum variation is for the Imperial Valley earthquake.

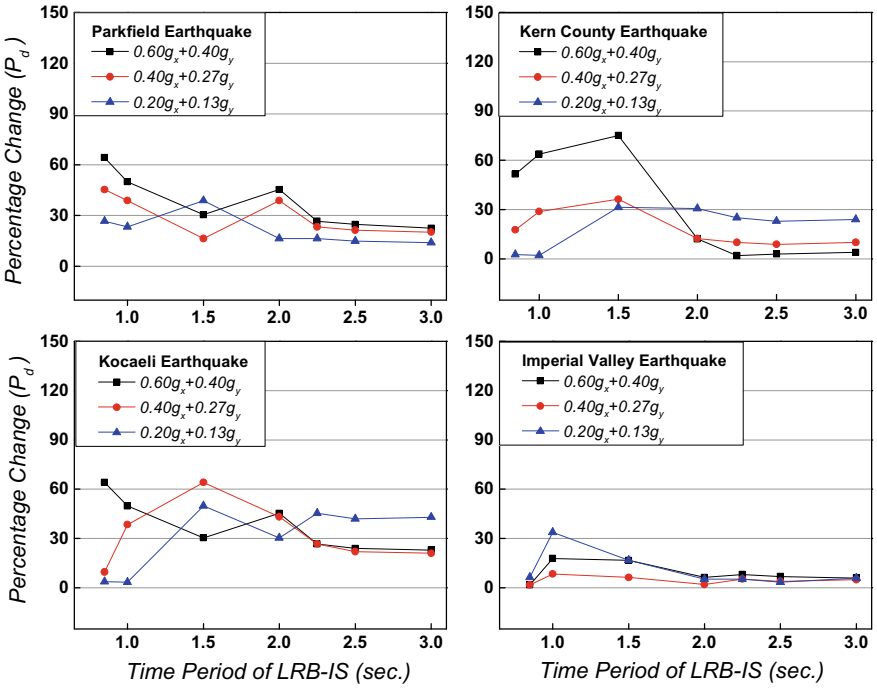

Fig. 22.8 Variation of percentage amplification in sloshing height with the time period of LRB isolator

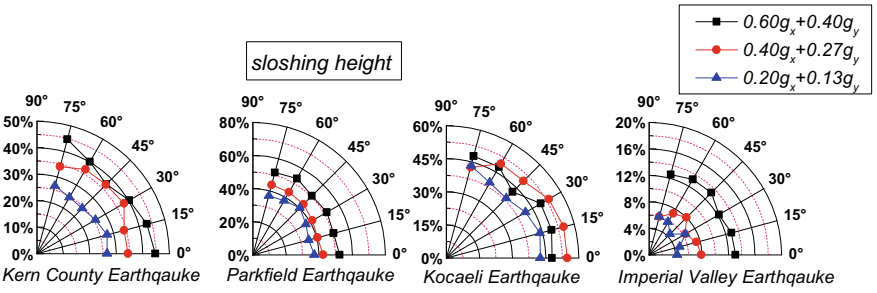

Fig. 22.9 Variation of percentage amplification in sloshing height with the time period of LRB isolator

22.5 Conclusions

The effectiveness of lead rubber bearing (LRB) in mitigation of the structural response and amplification of the sloshing height is studied by varying several important parameters. They include (i) effective time period of LRB isolator, (ii) the type of the ground motion, (iii) angle of incidence of the earthquake, and (iv) PGA. The

reductions in the response quantities are shear force, overturning moment, and hydrodynamic pressure. Also, it is known fact that seismic isolation tends to amplify the sloshing height which is also taken in the consideration for the present study. For the numerical study, a concrete LST with dimensions of 6 m ⊗ 6 m ⊗ 4.8 m is studied with a fluid height of 3.6 m and having five LRB base isolators attached to the base of the LST. The study reveals the following notable conclusions:

1. With the increase in the effective time period up to 2.5 s, decreases in the response quantities of interest and the enhancement in sloshing height usually increase, after which they appear to become stationary.
2. The maximum reduction of the order of 60–70% can be seen for the shear force and overturning moment at the optimum time period of the isolator system.
3. There is an ideal effective time period in which it is possible to obtain relatively high reductions in response quantities with much less amplification of the sloshing height; this effective time period is observed to be 2 s for the given study.
4. The effect of the type and PGA of ground motion are found to be an important factor for governing the responses.
5. Except for the drop in maximum hydrodynamic pressure and sloshing height amplification, the decrease in other response quantities is indifferent to the difference in the angle of incidence of the earthquake.

References

1. Housner GW (1963) The dynamic behavior of water tanks. Bull Seismol Soc Am 53:381–387
2. Housner GW (1957) Dynamic pressures on accelerated fluid containers. Bull Seismol Soc Am 47:15–35
3. Gupta RK, Hutchinson GL (1988) Free vibration analysis of liquid storage tanks. J Sound Vib 122:491–506
4. Sakal F, Nishimura M, Ogawa H (1984) Sloshing behavior of floating-roof oil storage tanks. Comput Struct 19:183–192
5. Gavrilyuk IP, Lukovsky IA, Timokha AN (2005) Linear and nonlinear sloshing in a circular conical tank. Fluid Dyn Res 37:399–429. https://doi.org/10.1016/j.fluiddyn.2005.08.004
6. Faltinsen OM, Rognebakke OF, Lukovsky IA, Timokha AN (2000) Multidimensional modal analysis of nonlinear sloshing in a rectangular tank with finite water depth. J Fluid Mech 407:201–234. https://doi.org/10.1017/S0022112099007569
7. Vern S, Shrimali MK, Bharti SD, Datta TK (2021) Seismic behavior of baffled liquid storage tank under far-field and near-field earthquake. In: Recent advances in computational mechanics and simulations. Springer, Singapore, pp 445–456. https://doi.org/10.1007/978-981-15-8138-0_34
8. Vern S, Shrimali MK, Bharti SD, Datta TK (2020) Impact of angle of incidence in rectangular liquid storage tanks. In: Technologies for sustainable development. CRC Press, pp 68–72. https://doi.org/10.1201/9780429321573-13
9. Vern S, Shrimali MK, Bharti SD, Datta TK (2021) Behavior of liquid storage tank under multi-directional excitation. In: Lecture Notes in Civil Engineering. Springer Science and Business Media Deutschland GmbH, pp 203–217. https://doi.org/10.1007/978-981-15-5235-9_16

10. Vern S, Shrimali MK, Bharti SD, Datta TK (accepted) Optimum passive control in the liquid storage tank by using multiple vertical baffles. Pract Period Struct Des Constr ASCE
11. Rawat A, Mittal V, Tanusree C, Matsagar V (2019) Earthquake induced sloshing and hydrodynamic in rigid liquid storage tanks analyed by coupled acoustic-structural and Euler-Lagrange methods. Thin-Walled Struct 333–346
12. Kirtas E, Rovithis E, Makra K (2020) On the modal response of an instrumented steel water-storage tank including soil-structure interaction. Soil Dyn Earthq Eng 135:106198. https://doi.org/10.1016/j.soildyn.2020.106198
13. Harry SW, Hampton FP (1999) Seismic response of isolated elevated water tanks. J Struct Eng 125:965–976
14. Shrimali MK, Jangid RS (2002) Non-linear seismic response of base-isolated liquid storage tanks to bi-directional excitation. Nucl Eng Des. https://doi.org/10.1016/S0029-5493(02)00134-6
15. Shrimali MK, Jangid RS (2003) Seismic response of isolated liquid storage tanks with elastomeric bearings. J Vib Control 2:1201–1218
16. Shrimali MK, Jangid RS (2003) Earthquake response of isolated elevated liquid storage steel tanks. J Constr Steel Res 59:1267–1288. https://doi.org/10.1016/S0143-974X(03)00066-X
17. Panchal VR, Jangid RS (2012) Behaviour of liquid storage tanks with VCFPS under near-fault ground motions. Struct Infrastruct Eng 8:71–88. https://doi.org/10.1080/15732470903300919
18. Shrimali MK, Jangid RS (2002) Seismic response of liquid storage tanks isolated by sliding bearings. Eng Struct 24:909–921. https://doi.org/10.1016/S0141-0296(02)00009-3
19. Liang B, Tang J (1994) xiang: Vibration studies of base-isolated liquid storage tanks. Comput Struct 52:1051–1059. https://doi.org/10.1016/0045-7949(94)90089-2
20. Son I-M, Kim J-M, Lee C (2019) Seismic soil-structure interaction analyses of LNG storage tanks depending on foundation type. J Comput Struct Eng Inst Korea 32:155–164. https://doi.org/10.7734/coseik.2019.32.3.155
21. Villegas-jim O, Tena-colunga A (1999) Dynamic design procedure for the design of base isolated, pp 1–8
22. Cheng X, Jing W, Gong L (2018) Dynamic responses of a sliding base-isolated RLSS considering free surface liquid sloshing. KSCE J Civ Eng 00:1–13. https://doi.org/10.1007/s12205-018-0154-z
23. Wen Y (1976) Method for random vibration of hysteretic systems. J Eng Mech Div 102:246–263
24. Bonet JL, Miguel PF, Fernandez MA, Romero ML (2006) Analytical approach to failure surfaces in reinforced and biaxial bending. J Struct Eng Eng 130:1133–1144. https://doi.org/10.1061/(ASCE)0733-9445(2004)130